Online Estimation of Lithium-Ion Battery State-of-Charge and Capacity with a Multiscale Filtering Technique

Chao Hu[1], Byeng D. Youn[2,*], Taejin Kim[2] and Jaesik Chung[3]

[1]*Department of Mechanical Engineering, University of Maryland, College Park, MD 20742, USA*
huchaost@umd.edu

[2]*School of Mechanical and Aerospace Engineering, Seoul National University, Seoul, 151-742, South Korea*
bdyoun@snu.ac.kr

[3] *PCTEST Engineering Laboratory, Columbia, Maryland 21045, USA*
anto@pctestlab.com

ABSTRACT

Real-time prediction of state-of-charge (SOC), state-of-health (SOH) and state-of-life (SOL) plays an essential role in many battery energy storage applications, such as electric vehicle (EV), hybrid electric vehicle (HEV) and smart power grid. However, among these three quantities, only the SOC has been thoroughly studies while there is still lack of rigorous research efforts on the other two quantities, SOH and SOL. Specially, real-time estimation of the SOH-relevant cell capacity by tracking readily available measurements (e.g., voltage, current and temperature) is still an open problem. Commonly used joint/dual extended Kalman filter (EKF) suffers from the lack of accuracy in the capacity estimation since (i) the cell voltage is the only measurable data for the SOC and capacity estimation and updates and (ii) the capacity is very weakly linked to the cell voltage. Furthermore, although the capacity is a slowly time-varying quantity that indicates cell state-of-health (SOH), the capacity estimation is generally performed on the same time-scale as the quickly time-varying SOC, resulting in high computational complexity. To resolve these difficulties, this paper proposes a multiscale framework with EKF for SOC and capacity estimation. The proposed framework comprises two ideas: (i) a multiscale framework to estimate SOC and capacity that exhibit time-scale separation and (ii) a state projection scheme for accurate and stable capacity estimation. Simulation and experimental results verify the effectiveness of our framework. †

* Corresponding author.

1. INTRODUCTION

As a battery cell ages, the cell capacity and resistance directly limit the pack performance through capacity and power fade, respectively (Plett, 2004a). These two degradation parameters are often used to quantify the cell state of health (SOH). Thus, it is important to accurately estimate these parameters to monitoring the present battery SOH and to predict the remaining useful life (RUL). Recent literature reports various approaches to estimate the SOH with a focus on the capacity estimation. Joint/dual extended Kalman filter (EKF) (Plett, 2004a) and unscented Kalman filter (Plett, 2006a) with an enhanced self-correcting model were proposed to simultaneously estimate the SOC, capacity and resistance. To improve the performance of joint/dual estimation, adaptive measurement noise models of the Kalman filter were recently developed to separate the sequence of SOC and capacity estimation (Lee et al., 2008). A physics-based single particle model was used to simulate the life cycling data of Li-ion cells and to study the physics of capacity fade (Zhang and White, 2008a; Zhang and White, 2008b). A Bayesian framework combining the relevance vector machine (RVM) and particle filter was proposed for prognostics (i.e., RUL prediction) of Li-ion battery cells (Saha et al., 2009). More recently, the particle filter with an empirical circuit model was used to predict the remaining useful lives for individual discharge cycles as well as for cycle life (Saha and Goebel, 2009).

Among these techniques, the joint/dual estimation technique is capable of real-time SOC and capacity estimation. Although it provides highly accurate SOC estimation, it suffers from the lack of accuracy in the capacity estimation since (i) the cell voltage is the only directly measurable data for the measurement updates in the SOC and capacity estimation (indirectly measurable data such as electrochemical impedance

require additional devices) and (ii) the capacity is very weakly linked to the cell voltage. Due to the strong correlation between the SOC and capacity, inaccurate capacity estimation may further lead to inaccurate SOC estimation and vice versa. Furthermore, although the capacity is a slowly time-varying quantity that indicates cell state-of-health (SOH), the capacity estimation is generally performed on the same time-scale as the quickly time-varying SOC, resulting in high computational complexity. To resolve these difficulties, this paper proposes a multiscale framework with EKF for SOC and capacity estimation. The proposed framework comprises two ideas: (i) a multiscale framework to estimate SOC and capacity that exhibit time-scale separation and (ii) a state projection scheme for accurate and stable capacity estimation. It is noted that the multiscale framework is generic since it can be used to achieve highly-confident health prognostics for any engineered system with multiple time-scales.

This paper is organized as follows. Section 2 describes the discrete-time state-space model of an engineered system with multiple time-scales. Section 3 reviews the numerical formulation and implementation of the dual EKF method. Section 4 resents the proposed multiscale framework with EKF and introduces the state projection scheme. The proposed ideas are applied to a Li-ion battery system to estimate SOC and capacity in Section 5. Section 6 contains simulation and experimental results of this application. The paper is concluded in Section 7.

2. SYSTEM DESCRIPTION

To make the discussion more concrete, we will use discrete-time state-space models with multiple time-scales. Without loss of generality, we assume the system has two time-scales: the macro and micro time-scales. System quantities on the macro time-scale tend to vary slowly over time while system quantities on the micro time-scale exhibit fast variation over time. The former are referred to as the model parameters of the system while the latter are called the states of the system. We then begin by defining the nonlinear state-space model considered in this work as

$$\begin{aligned} &\text{Transition:} && \mathbf{x}_{k,l+1} = \mathbf{F}\left(\mathbf{x}_{k,l}, \mathbf{u}_{k,l}, \boldsymbol{\theta}_k\right) + \mathbf{w}_{k,l}, \\ & && \boldsymbol{\theta}_{k+1} = \boldsymbol{\theta}_k + \mathbf{r}_k, \\ &\text{Measurement:} && \mathbf{y}_{k,l} = \mathbf{G}\left(\mathbf{x}_{k,l}, \mathbf{u}_{k,l}, \boldsymbol{\theta}_k\right) + \mathbf{v}_{k,l} \end{aligned} \tag{1}$$

where $\mathbf{x}_{k,l}$ is the vector of system states at the time $t_{k,l} = t_{k,0} + l \cdot T$, for $1 \le l \le L$, with T being a fixed time step between two adjacent measurement points, and k and l being the indices of macro and micro time-scales, respectively; $\boldsymbol{\theta}_k$ is the vector of system model parameters at the time $t_{k,0}$; $\mathbf{u}_{k,l}$ is the vector of observed exogenous inputs; $\mathbf{y}_{k,l}$ is the vector of system observations (or measurements); $\mathbf{w}_{k,l}$ and $\mathbf{r}_k$ are the vectors of process noise for states and model parameters, respectively; $\mathbf{v}_{k,l}$ is the vectors of measurement noise; $\mathbf{F}(\bullet,\bullet,\bullet)$ and $\mathbf{G}(\bullet,\bullet,\bullet)$ are the state transition and measurement functions, respectively. Note that L represents the level of time-scale separation and that $\mathbf{x}_{k,0} = \mathbf{x}_{k-1,L}$. With the system defined, we aim at estimating both the system states $\mathbf{x}$ and model parameters $\boldsymbol{\theta}$ from the noisy observations $\mathbf{y}$.

Let's take the battery system as an example. In the battery system, the system state x refers to the SOC, which changes very rapidly and may transverse the entire range 100%-0% within minutes. The system model parameter θ represents the cell capacity which tends to vary very slowly and typically decreases 1.0% or less in a month with regular use. The state transition equation $F(\bullet,\bullet,\bullet)$ models the variation of SOC over time while the cell dynamic model $G(\bullet,\bullet,\bullet)$ relates the measured cell terminal voltage y with the unmeasured state (SOC) and model parameter (capacity) and the measured exogenous input u being the cell current. Given the system's state-space model in Eq. (1) and knowledge of the measured input/output signals (cell current/cell terminal voltage), we are interested in estimating the unmeasured state (SOC) and model parameter (capacity) in real-time and in a dynamic driving environment.

3. REVIEW OF DUAL EXTENDED KALMAN FILTER METHOD

The dual extended Kalman filter (EKF) method is a commonly used technique to simultaneously estimate the states and model parameters (Haykin, 2001). The essence of the dual EKF method is to combine the state and weight EKFs with the state EKF estimating the system states and the weight EKF estimating the system model parameters. In the algorithm, two EKFs are run concurrently and, at every time step when observations are available, the state EKF estimates the states using the current model parameter estimates from the weight EKF while the weight EKF estimates the model parameters using the current state estimates from the state EKF. This section gives a brief review of the dual EKF method. Section 3.1 presents the numerical formulation of the dual EKF method and the numerical implementation of the recursive derivative computation is described in Section 3.2.

3.1 Numerical Formulation: Dual Estimation

The algorithm of the dual EKF for the system described in Eq. (1) is summarized in Table 1. Since the dual EKF does not take into account the time-scale separation, $\boldsymbol{\theta}_k$ is estimated on the micro time-scale. To reflect this, we use the notations $\boldsymbol{\theta}_{k,l}$ and $\mathbf{r}_{k,l}$ to replace $\boldsymbol{\theta}_k$ and $\mathbf{r}_k$, respectively. Also note that, to be consistent with the system description in Eq. (1), we use two time

indices k and l to present the dual EKF algorithm and this presentation is equivalent to a simpler version in (Wan and Nelson, 2001) with only one time index l.

The algorithm is initialized by setting the model parameters $\boldsymbol{\theta}$ and states $\mathbf{x}$ to the best guesses based on the prior information. The covariance matrices $\boldsymbol{\Sigma}_{\boldsymbol{\theta}}$ and $\boldsymbol{\Sigma}_{\mathbf{x}}$ of estimation errors are also initialized based on the prior information. At each measurement time step, the time- and measurement-updates of the state and weight EKFs are performed. In the time-update, the state and parameter estimates from the previous measurement time step are propagated forward in time according to the transition equations in Eq. (1). The current state and parameter estimates are set equal to these propagated estimates and the error uncertainties are increased due to the addition of process noise $\mathbf{w}$ and $\mathbf{r}$. In the measurement update, the measurement at the current time step is compared with the predicted model outputs based on the current state and parameter estimates and the differences are used to adapt the current estimates.

3.2 Numerical Implementation: Recursive Derivative Computation

The dual EKF method, which adapts the states and parameters using two concurrently running EKFs, has a recursive architecture associated with the computation of $\mathbf{C}_{k,l}^{\boldsymbol{\theta}}$ in the weight filter. The computation of $\mathbf{C}_{k,l}^{\boldsymbol{\theta}}$ involves a total derivative of the measurement function with respect to the parameters $\boldsymbol{\theta}$ as

$$\mathbf{C}_{k,l}^{\boldsymbol{\theta}} = \left. \frac{d\mathbf{G}\left(\hat{\mathbf{x}}_{k,l}^{-}, \mathbf{u}_{k,l}, \boldsymbol{\theta}\right)}{d\boldsymbol{\theta}} \right|_{\boldsymbol{\theta}=\hat{\boldsymbol{\theta}}_{k,l}^{-}}. \tag{2}$$

This computation requires a recursive routine similar to a real-time recursive learning (Williams and Zipser, 1989). Decomposing the total derivative into partial derivatives and propagating the states back in time results in the recursive equations

$$\frac{d\mathbf{G}\left(\hat{\mathbf{x}}_{k,l}^{-}, \mathbf{u}_{k,l}, \boldsymbol{\theta}\right)}{d\boldsymbol{\theta}} = \frac{\partial \mathbf{G}\left(\hat{\mathbf{x}}_{k,l}^{-}, \mathbf{u}_{k,l}, \boldsymbol{\theta}\right)}{\partial \boldsymbol{\theta}} + \frac{\partial \mathbf{G}\left(\hat{\mathbf{x}}_{k,l}^{-}, \mathbf{u}_{k,l}, \boldsymbol{\theta}\right)}{\partial \hat{\mathbf{x}}_{k,l}^{-}} \frac{d\hat{\mathbf{x}}_{k,l}^{-}}{d\boldsymbol{\theta}}, \tag{3}$$

$$\frac{d\hat{\mathbf{x}}_{k,l}^{-}}{d\boldsymbol{\theta}} = \frac{\partial \mathbf{F}\left(\hat{\mathbf{x}}_{k,l-1}, \mathbf{u}_{k,l-1}, \boldsymbol{\theta}\right)}{\partial \boldsymbol{\theta}} + \frac{\partial \mathbf{F}\left(\hat{\mathbf{x}}_{k,l-1}, \mathbf{u}_{k,l-1}, \boldsymbol{\theta}\right)}{\partial \hat{\mathbf{x}}_{k,l-1}} \frac{d\hat{\mathbf{x}}_{k,l-1}}{d\boldsymbol{\theta}}, \tag{4}$$

$$\frac{d\hat{\mathbf{x}}_{k,l-1}}{d\boldsymbol{\theta}} = \frac{d\hat{\mathbf{x}}_{k,l-1}^{-}}{d\boldsymbol{\theta}} - \mathbf{K}_{k,l-1}^{\mathbf{x}} \frac{d\mathbf{G}\left(\hat{\mathbf{x}}_{k,l-1}^{-}, \mathbf{u}_{k,l-1}, \boldsymbol{\theta}\right)}{d\boldsymbol{\theta}} + \frac{\partial \mathbf{K}_{k,l-1}^{\mathbf{x}}}{\partial \boldsymbol{\theta}} \left[\mathbf{y}_{k,l-1} - \mathbf{G}\left(\hat{\mathbf{x}}_{k,l-1}^{-}, \mathbf{u}_{k,l-1}, \boldsymbol{\theta}\right)\right]. \tag{5}$$

The last term in Eq. (5) can be set to zero with the assumption that $\mathbf{K}_{k,l}^{\mathbf{x}}$ is not dependent on $\boldsymbol{\theta}$. Indeed, since $\mathbf{K}_{k,l}^{\mathbf{x}}$ is often very weakly dependent on $\boldsymbol{\theta}$, the extra computational effort to consider this dependence is not worth the improvement in performance. Therefore, we drop the last term in Eq. (5) in this study. Then the three total derivatives can be computed in a recursive manner with initial values set as zeros. It noted that the partial derivatives of the transition and measurement functions with respect to the states $\mathbf{x}$ and parameters $\boldsymbol{\theta}$ can be easily computed with the explicitly given function forms.

4. A MULTISCALE FRAMEWORK WITH EXTENDED KALMAN FILTER

As discussed in Section 3, the dual EKF method estimates both the states and parameters on the same time-scale. However, for systems that exhibit the time-scale separation, it is natural and desirable to adapt the slowly time-varying parameters on the macro time-scale while keeping the estimation of the fast time-varying states on the micro time-scale. This section is dedicated to the discussion of this multiscale framework. Section 4.1 presents the numerical formulation of the multiscale framework and the numerical implementation of the recursive derivative computation is described in Section 4.2.

4.1 Numerical Formulation: Multiscale Estimation

As opposed to the dual estimation, we intend to derive a multiscale estimation which allows for a time-scale separation in the state and parameter estimations. More specifically, we aim at estimating the slowly time-varying model parameters on the macro time-scale and, at the same time, intend to keep the estimation of fast time-varying states on the micro time-scale to utilize all the measurements. For these purposes, we derive the so-called micro and macro EKFs running on the micro and macro time-scales, respectively. Note that, the micro time-scale here refers to the time-scale on which system states exhibit fast variation while the macro time-scale refers to the one on which system model parameters tend to vary slowly. For example, in the battery system, the SOC, as a system state, changes every second, which suggests the micro time-scale is approximately one second. In contrast, the cell capacity, as a system model parameter, typically decreases 1.0% or less in a month with regular use, resulting in the macro time-scale being approximately one day or so. In the micro EKF, similar to the state EKF in the dual estimation, the states are estimated based on measurements $\mathbf{y}$. In the macro EKF, the measurements used to adapt the model parameters are the estimated states from the micro EKF.

Table 1 Algorithm of dual extended Kalman filter (Wan and Nelson, 2001)

Initialization

$$\hat{\boldsymbol{\theta}}_{0,0} = E\left[\hat{\boldsymbol{\theta}}_{0,0}\right],\ \ \boldsymbol{\Sigma}_{\boldsymbol{\theta}_{k,l}} = E\left[\left(\boldsymbol{\theta}_{0,0}-\hat{\boldsymbol{\theta}}_{0,0}\right)\left(\boldsymbol{\theta}_{0,0}-\hat{\boldsymbol{\theta}}_{0,0}\right)^{\mathrm{T}}\right],$$
$$\hat{\mathbf{x}}_{0,0} = E\left[\mathbf{x}_{0,0}\right],\ \ \boldsymbol{\Sigma}_{\mathbf{x}_{k,l}} = E\left[\left(\mathbf{x}_{0,0}-\hat{\mathbf{x}}_{0,0}\right)\left(\mathbf{x}_{0,0}-\hat{\mathbf{x}}_{0,0}\right)^{\mathrm{T}}\right]. \tag{6}$$

For $k\in\{1,\ldots,\infty\}$, $l\in\{1,\ldots,L\}$, compute

Time-update equations for the weight filter

$$\hat{\boldsymbol{\theta}}^{-}_{k,l} = \hat{\boldsymbol{\theta}}_{k,l-1},\qquad \boldsymbol{\Sigma}^{-}_{\boldsymbol{\theta}_{k,l}} = \boldsymbol{\Sigma}_{\boldsymbol{\theta}_{k,l-1}} + \boldsymbol{\Sigma}_{\mathbf{r}_{k,l-1}}. \tag{7}$$

Time-update equations for the state filter

$$\hat{\mathbf{x}}^{-}_{k,l} = \mathbf{F}\left(\hat{\mathbf{x}}_{k,l-1},\mathbf{u}_{k,l-1},\hat{\boldsymbol{\theta}}^{-}_{k,l}\right),\ \ \boldsymbol{\Sigma}^{-}_{\mathbf{x}_{k,l}} = \mathbf{A}_{k,l-1}\boldsymbol{\Sigma}_{\mathbf{x}_{k,l-1}}\mathbf{A}^{\mathrm{T}}_{k,l-1} + \boldsymbol{\Sigma}_{\mathbf{w}_{k,l-1}}. \tag{8}$$

Measurement-update equations for the state filter

$$\mathbf{K}^{\mathbf{x}}_{k,l} = \boldsymbol{\Sigma}^{-}_{\mathbf{x}_{k,l}}\left(\mathbf{C}^{\mathbf{x}}_{k,l}\right)^{\mathrm{T}}\left[\mathbf{C}^{\mathbf{x}}_{k,l}\boldsymbol{\Sigma}^{-}_{\mathbf{x}_{k,l}}\left(\mathbf{C}^{\mathbf{x}}_{k,l}\right)^{\mathrm{T}} + \boldsymbol{\Sigma}_{\mathbf{v}_{k,l}}\right]^{-1}. \tag{9}$$

$$\hat{\mathbf{x}}_{k,l} = \hat{\mathbf{x}}^{-}_{k,l} + \mathbf{K}^{\mathbf{x}}_{k,l}\left[\mathbf{y}_{k,l} - \mathbf{G}\left(\hat{\mathbf{x}}^{-}_{k,l},\mathbf{u}_{k,l},\hat{\boldsymbol{\theta}}^{-}_{k,l}\right)\right],\ \ \boldsymbol{\Sigma}_{\mathbf{x}_{k,l}} = \left(\mathbf{I}-\mathbf{K}^{\mathbf{x}}_{k,l}\mathbf{C}^{\mathbf{x}}_{k,l}\right)\boldsymbol{\Sigma}^{-}_{\mathbf{x}_{k,l}}. \tag{10}$$

Measurement-update equations for the weight filter

$$\mathbf{K}^{\boldsymbol{\theta}}_{k,l} = \boldsymbol{\Sigma}^{-}_{\boldsymbol{\theta}_{k,l}}\left(\mathbf{C}^{\boldsymbol{\theta}}_{k,l}\right)^{\mathrm{T}}\left[\mathbf{C}^{\boldsymbol{\theta}}_{k,l}\boldsymbol{\Sigma}^{-}_{\boldsymbol{\theta}_{k,l}}\left(\mathbf{C}^{\boldsymbol{\theta}}_{k,l}\right)^{\mathrm{T}} + \boldsymbol{\Sigma}_{\mathbf{n}_{k,l}}\right]^{-1}. \tag{11}$$

$$\hat{\boldsymbol{\theta}}_{k,l} = \hat{\boldsymbol{\theta}}^{-}_{k,l} + \mathbf{K}^{\boldsymbol{\theta}}_{k,l}\left[\mathbf{y}_{k,l} - \mathbf{G}\left(\hat{\mathbf{x}}^{-}_{k,l},\mathbf{u}_{k,l},\hat{\boldsymbol{\theta}}^{-}_{k,l}\right)\right],\ \ \boldsymbol{\Sigma}_{\boldsymbol{\theta}_{k,l}} = \left(\mathbf{I}-\mathbf{K}^{\boldsymbol{\theta}}_{k,l}\mathbf{C}^{\boldsymbol{\theta}}_{k,l}\right)\boldsymbol{\Sigma}^{-}_{\boldsymbol{\theta}_{k,l}}. \tag{12}$$

where

$$\mathbf{A}_{k,l-1} = \left.\frac{\partial\mathbf{F}\left(\mathbf{x},\mathbf{u}_{k,l-1},\hat{\boldsymbol{\theta}}^{-}_{k,l}\right)}{\partial\mathbf{x}}\right|_{\mathbf{x}=\hat{\mathbf{x}}_{k,l-1}},\ \ \mathbf{C}^{\mathbf{x}}_{k,l} = \left.\frac{\partial\mathbf{G}\left(\mathbf{x},\mathbf{u}_{k,l},\hat{\boldsymbol{\theta}}^{-}_{k,l}\right)}{\partial\mathbf{x}}\right|_{\mathbf{x}=\hat{\mathbf{x}}^{-}_{k,l}},\ \ \mathbf{C}^{\boldsymbol{\theta}}_{k,l} = \left.\frac{d\mathbf{G}\left(\hat{\mathbf{x}}^{-}_{k,l},\mathbf{u}_{k,l},\boldsymbol{\theta}\right)}{d\boldsymbol{\theta}}\right|_{\boldsymbol{\theta}=\hat{\boldsymbol{\theta}}^{-}_{k,l}}. \tag{13}$$

A state projection scheme is introduced to project the state through the macro time step, expressed as

$$\mathbf{x}_{k-1,L} = \mathbf{F}_{0\to L}\left(\mathbf{x}_{k-1,0},\mathbf{u}_{k-1,0:L-1},\boldsymbol{\theta}_{k-1}\right) \tag{14}$$

where the state projection function $\mathbf{F}_{0\to L}(\bullet,\bullet,\bullet)$ can be expressed as a nested form of the state transition function $\mathbf{F}(\bullet,\bullet,\bullet)$. It is noted that the computational effort involved in computing $\mathbf{F}_{0\to L}(\bullet,\bullet,\bullet)$ is negligible compared to the time- and measurement-updates conducted in L micro time steps.

The algorithm of the multiscale framework for the system described in Eq. (1) is summarized in Table 2. Note that, in contrast to the dual EKF algorithms in Table 1, we only use the macro time-scale index k to present the macro EKF since it estimates the parameters on the macro time-scale. The algorithm is initialized by setting the model parameters $\boldsymbol{\theta}$ and states $\mathbf{x}$ to the best guesses based on the prior information. The covariance matrices $\boldsymbol{\Sigma}_{\boldsymbol{\theta}}$ and $\boldsymbol{\Sigma}_{\mathbf{x}}$ of estimation errors are also initialized based on the prior information. At each time step on the macro time-scale, the time- and measurement-updates of the macro EKF is performed while, at each time step on the micro time-scale, the time- and measurement-updates of the micro EKF is performed. In the measurement-update of the macro EKF, the state estimate at the previous macro time step from the micro EKF is projected through the macro time step according to the state projection equation in Eq. (14). Then the state estimates at the current macro time step from the micro EKF are compared with the projected estimates and the differences are used to adapt the current parameter estimates.

Table 2 Algorithm of a multiscale framework with extended Kalman filter

Initialization

$$\hat{\boldsymbol{\theta}}_0 = E\left[\hat{\boldsymbol{\theta}}_0\right], \quad \boldsymbol{\Sigma}_{\boldsymbol{\theta}_{k,l}} = E\left[\left(\boldsymbol{\theta}_0 - \hat{\boldsymbol{\theta}}_0\right)\left(\boldsymbol{\theta}_0 - \hat{\boldsymbol{\theta}}_0\right)^{\mathrm{T}}\right],$$
$$\hat{\mathbf{x}}_{0,0} = E\left[\mathbf{x}_{0,0}\right], \quad \boldsymbol{\Sigma}_{\mathbf{x}_{k,l}} = E\left[\left(\mathbf{x}_{0,0} - \hat{\mathbf{x}}_{0,0}\right)\left(\mathbf{x}_{0,0} - \hat{\mathbf{x}}_{0,0}\right)^{\mathrm{T}}\right]. \tag{15}$$

For $k \in \{1, \ldots, \infty\}$, compute

Time-update equations for the macro EKF

$$\hat{\boldsymbol{\theta}}_k^- = \hat{\boldsymbol{\theta}}_{k-1}, \qquad \boldsymbol{\Sigma}_{\boldsymbol{\theta}_k}^- = \boldsymbol{\Sigma}_{\boldsymbol{\theta}_{k-1}} + \boldsymbol{\Sigma}_{\mathbf{r}_{k-1}}. \tag{16}$$

State projection equation for the macro EKF

$$\tilde{\mathbf{x}}_{k-1,L} = \mathbf{F}_{0\to L}\left(\hat{\mathbf{x}}_{k-1,0}, \mathbf{u}_{k-1,0:L-1}, \hat{\boldsymbol{\theta}}_k^-\right). \tag{17}$$

Measurement-update equations for the macro EKF

$$\mathbf{K}_k^{\boldsymbol{\theta}} = \boldsymbol{\Sigma}_{\boldsymbol{\theta}_k}^- \left(\mathbf{C}_k^{\boldsymbol{\theta}}\right)^{\mathrm{T}} \left[\mathbf{C}_k^{\boldsymbol{\theta}} \boldsymbol{\Sigma}_{\boldsymbol{\theta}_k}^- \left(\mathbf{C}_k^{\boldsymbol{\theta}}\right)^{\mathrm{T}} + \boldsymbol{\Sigma}_{\mathbf{n}_k}\right]^{-1}. \tag{18}$$

$$\hat{\boldsymbol{\theta}}_k = \hat{\boldsymbol{\theta}}_k^- + \mathbf{K}_k^{\boldsymbol{\theta}}\left[\hat{\mathbf{x}}_{k-1,L} - \tilde{\mathbf{x}}_{k-1,L}\right], \qquad \boldsymbol{\Sigma}_{\boldsymbol{\theta}_k} = \left(\mathbf{I} - \mathbf{K}_k^{\boldsymbol{\theta}} \mathbf{C}_k^{\boldsymbol{\theta}}\right) \boldsymbol{\Sigma}_{\boldsymbol{\theta}_k}^-. \tag{19}$$

For $l \in \{1, \ldots, L\}$, compute

Time-update equations for the micro EKF

$$\hat{\mathbf{x}}_{k,l}^- = \mathbf{F}\left(\hat{\mathbf{x}}_{k,l-1}, \mathbf{u}_{k,l-1}, \hat{\boldsymbol{\theta}}_{k-1}\right), \ \boldsymbol{\Sigma}_{\mathbf{x}_{k,l}}^- = \mathbf{A}_{k,l-1} \boldsymbol{\Sigma}_{\mathbf{x}_{k,l-1}} \mathbf{A}_{k,l-1}^{\mathrm{T}} + \boldsymbol{\Sigma}_{\mathbf{w}_{k,l-1}}. \tag{20}$$

Measurement-update equations for the micro EKF

$$\mathbf{K}_{k,l}^{\mathbf{x}} = \boldsymbol{\Sigma}_{\mathbf{x}_{k,l}}^- \left(\mathbf{C}_{k,l}^{\mathbf{x}}\right)^{\mathrm{T}} \left[\mathbf{C}_{k,l}^{\mathbf{x}} \boldsymbol{\Sigma}_{\mathbf{x}_{k,l}}^- \left(\mathbf{C}_{k,l}^{\mathbf{x}}\right)^{\mathrm{T}} + \boldsymbol{\Sigma}_{\mathbf{v}_{k,l}}\right]^{-1}. \tag{21}$$

$$\hat{\mathbf{x}}_{k,l} = \hat{\mathbf{x}}_{k,l}^- + \mathbf{K}_{k,l}^{\mathbf{x}}\left[\mathbf{y}_{k,l} - \mathbf{G}\left(\hat{\mathbf{x}}_{k,l}^-, \mathbf{u}_{k,l}, \hat{\boldsymbol{\theta}}_{k-1}\right)\right], \ \boldsymbol{\Sigma}_{\mathbf{x}_{k,l}} = \left(\mathbf{I} - \mathbf{K}_{k,l}^{\mathbf{x}} \mathbf{C}_{k,l}^{\mathbf{x}}\right) \boldsymbol{\Sigma}_{\mathbf{x}_{k,l}}^-. \tag{22}$$

where

$$\mathbf{A}_{k,l-1} = \left.\frac{\partial \mathbf{F}\left(\mathbf{x}, \mathbf{u}_{k,l-1}, \hat{\boldsymbol{\theta}}_{k-1}\right)}{\partial \mathbf{x}}\right|_{\mathbf{x}=\hat{\mathbf{x}}_{k,l-1}}, \ \mathbf{C}_{k,l}^{\mathbf{x}} = \left.\frac{\partial \mathbf{G}\left(\mathbf{x}, \mathbf{u}_{k,l}, \hat{\boldsymbol{\theta}}_{k-1}\right)}{\partial \mathbf{x}}\right|_{\mathbf{x}=\hat{\mathbf{x}}_{k,l}^-}, \ \mathbf{C}_k^{\boldsymbol{\theta}} = \left.\frac{d\mathbf{F}_{0\to L}\left(\hat{\mathbf{x}}_{k-1,0}, \mathbf{u}_{k-1,0:L-1}, \boldsymbol{\theta}\right)}{d\boldsymbol{\theta}}\right|_{\boldsymbol{\theta}=\hat{\boldsymbol{\theta}}_k^-}. \tag{23}$$

4.2 Numerical Implementation: Recursive Derivative Computation

In the multiscale framework, the computation of $\mathbf{C}_k^{\boldsymbol{\theta}}$ in the macro EKF involves a total derivative of the state projection function with respect to the parameters $\boldsymbol{\theta}$ as

$$\mathbf{C}_k^{\boldsymbol{\theta}} = \left.\frac{d\mathbf{F}_{0\to L}\left(\hat{\mathbf{x}}_{k-1,0}, \mathbf{u}_{k-1,0:L-1}, \boldsymbol{\theta}\right)}{d\boldsymbol{\theta}}\right|_{\boldsymbol{\theta}=\hat{\boldsymbol{\theta}}_k^-}. \tag{24}$$

Similar to the total derivative in Eq. (2), this computation also requires a recursive routine. Decomposing the total derivative into partial derivatives, we then obtain the following equation

$$\frac{d\mathbf{F}_{0\to L}\left(\hat{\mathbf{x}}_{k-1,0}, \mathbf{u}_{k-1,0:L-1}, \boldsymbol{\theta}\right)}{d\boldsymbol{\theta}} = \frac{\partial \mathbf{F}_{0\to L}\left(\hat{\mathbf{x}}_{k-1,0}, \mathbf{u}_{k-1,0:L-1}, \boldsymbol{\theta}\right)}{\partial \boldsymbol{\theta}} + \frac{\partial \mathbf{F}_{0\to L}\left(\hat{\mathbf{x}}_{k-1,0}, \mathbf{u}_{k-1,0:L-1}, \boldsymbol{\theta}\right)}{\partial \hat{\mathbf{x}}_{k-1,0}} \frac{d\hat{\mathbf{x}}_{k-1,0}}{d\boldsymbol{\theta}}. \tag{25}$$

The total derivative in the last term can be obtained by using the recursive equations Eqs. (3)-(5).

5. APPLICATION TO LI-ION BATTERY SYSTEM

In this section, we use the proposed framework to estimate the SOC and capacity in a Li-ion battery system. When applied to the battery system, the multiscale framework can be treated as a hybrid of coulomb counting and adaptive filtering techniques and comprises two new ideas: (i) a multiscale framework to estimate SOC and capacity that exhibit time-scale separation and (ii) a state projection scheme for accurate and stable capacity estimation. Section 5.1 presents the discrete-time cell dynamic model used in this study. Section 5.2 presents the multiscale estimation of SOC and capacity.

5.1 Discrete-Time Cell Dynamic Model

In order to execute the time-update in the micro and macro EKFs, we need a state transition model that propagate the SOC forward in time. In order to execute the measurement-update in the micro-EKF, we need a "discrete-time cell dynamic model" that relates the SOC to the cell voltage. Here we employ the enhanced self-correcting (ESC) model which considers the effects of open circuit voltage (OCV), internal resistance, voltage time constants and hysteresis (Plett, 2004a). The effects of voltage time constants and hysteresis in the ESC model can be expressed as (Plett, 2004a)

$$\begin{bmatrix} f_{k,l+1} \\ h_{k,l+1} \end{bmatrix} = \begin{bmatrix} \mathrm{diag}(\boldsymbol{\alpha}) & 0 \\ 0 & \varphi(i_{k,l+1}) \end{bmatrix} \begin{bmatrix} f_{k,l} \\ h_{k,l} \end{bmatrix} + \begin{bmatrix} 1 & 0 \\ 0 & 1-\varphi(i_{k,l+1}) \end{bmatrix} \begin{bmatrix} i_{k,l} \\ M(x,\dot{x}) \end{bmatrix} \tag{26}$$

$$\varphi(i_{k,l+1}) = \exp\left(-\left|\frac{\eta_i \cdot i_{k,l} \cdot \gamma \cdot T}{C_k}\right|\right) \tag{27}$$

where x is the SOC, f the filter state, h the hysteresis voltage, $\boldsymbol{\alpha}$ the vector of filter pole locations, γ the hysteresis rate constant, i the current, $M(\cdot,\cdot)$ maximum hysteresis, η_i the Coulombic efficiency, T the length of measurement interval, C the nominal capacity. We then obtain the state transition and measurement equations as

$$\begin{aligned} x_{k,l+1} &= F(x_{k,l}, i_{k,l}, C_k) \\ &= x_{k,l} - \frac{\eta_i \cdot T \cdot i_{k,l}}{C_k}, \\ y_{k,l+1} &= G(x_{k,l}, i_{k,l}, C_k) \\ &= \mathrm{OCV}(z_k) - i_{k,l} \cdot R + h_{k,l+1} + S \cdot f_{k,l+1}. \end{aligned} \tag{28}$$

where OCV is the open circuit voltage, y_k the predicted cell terminal voltage, R the cell resistance, S a vector of constants that blend the time constant states together in the output.

5.2 Multiscale Estimation of SOC and Capacity

We then begin to introduce the multiscale framework with EKF for the Li-ion battery system by drawing a flowchart in Figure 1, where T is a fixed time step between two adjacent measurement points, $x_{k,l}$ is the SOC estimate at the time $t_{k,l} = t_{k,0} + l \cdot T$., for $1 \le l \le L$ (k and l are the indices of macro and micro time-scales, respectively), y and i are the cell voltage and current measurements, and C is the cell capacity estimate.

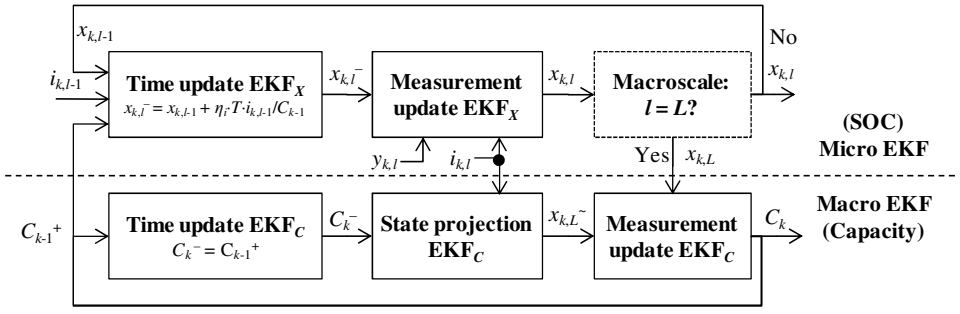

Figure 1: Flowchart of a multiscale framework with EKF for battery SOC and capacity estimation.

The framework consists of two EKFs running in parallel: the top one (micro EKF) adapting the SOC in the micro time-scale and the bottom one (macro EKF) adapting the capacity in the macro time-scale. The micro EKF sends the SOC estimate to the macro EKF and receives the capacity estimate from the macro EKF. In what follows, we intend to elaborate on the key technical component of the multiscale framework, the macro EKF, which consists of the following recursively executed procedures (see Figure 2):

Step 1: At the macro time step k, the capacity transition step, also known as the time update step, computes the expected capacity and its variance based

on the updated estimates at the time step $k-1$, expressed as

$$C_k^- = C_{k-1}^+, \qquad \Sigma_{C_k}^- = \Sigma_{C_{k-1}}^+ + \Sigma_{r_{k-1}}. \tag{29}$$

For a stable system, the capacity variance term tends to decrease over time with the measurement update to be detailed in the subsequent step. However, the process noise term always increases the uncertainty of the capacity estimate due to the addition of unpredictable process noise. To clearly illustrate the idea, we intend to classify the capacity estimates into three cases (see Figure 1): a larger estimate $C_{k-1}^{(L)}$, an accurate estimate $C_{k-1}^{(N)}$, and a smaller estimate $C_{k-1}^{(S)}$.

Step 2: Based on the capacity estimate C_k^-, the state projection scheme projects the SOC through the macro time step, expressed as a state projection equation derived from Eqs. (14) and (28)

$$x_{k,L} = x_{k,0} + \frac{\eta \cdot T}{C_k^-} \cdot \sum_{j=0}^{L-1} i_{k,j}. \tag{30}$$

As can be seen in Figure 2:, the projected SOCs exhibit large deviations from their true value (from micro EKF), which suggests a magnified effect of the capacity on the SOC.

Step 3: Following the state projection step, the difference between the projected SOC and the estimated SOC by the micro EKF is used to update the capacity estimate, known as the measurement update. It is noted that the measurement update requires accurate SOC estimates which can be obtained from the micro EKF. The updated capacity estimate equals the predicted capacity estimate in *Step 1* plus a correction factor, expressed as

$$\begin{aligned} C_k^+ &= C_k^- + K_k^C \left[\hat{\mathbf{x}}_{k,L} - \tilde{\mathbf{x}}_{k,L} \right], \\ \Sigma_{C_k}^+ &= \left(1 - K_k^C C_k^C\right) \Sigma_{C_k}^-. \end{aligned} \tag{31}$$

where the Kalman gain K_k^C and the total derivative C_k^C can be estimated using Eqs. (18) and (23), respectively.

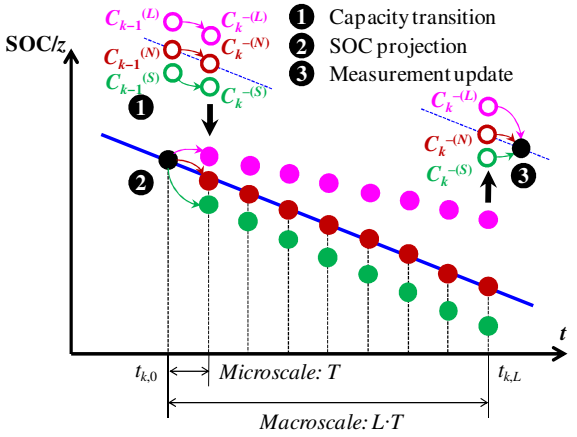

Figure 2: Procedures of capacity estimation in macro EKF.

5.3 Remarks on Mutiscale Framework

We note that the proposed framework decouples the SOC and capacity estimation in terms of both the measurement and time-scale, with an aim to avoid the concurrent SOC and capacity estimation relying on the only measurement (cell terminal voltage) in the dual EKF (Plett, 2004a). In fact, the very motivation of this work lies in the fact that the coupled estimation in the dual EKF falls short in the way of achieving stable capacity estimation, precisely because it is difficult to distinguish the effects of two states (SOC and capacity) on the only measurement (cell terminal voltage), especially in the case of the micro time-scale where the capacity only has a very small influence on the SOC. Regarding the measurement decoupling, the multiscale framework uses the cell terminal voltage exclusively as the measurement for adapting the SOC (micro EKF) which in turn serves as the measurement to adapt the capacity (macro EKF). Regarding the time-scale decoupling, the state projection using the coulomb counting in Eq. (30) significantly magnifies the effect of the capacity on the SOC, i.e., that the capacity affects the SOC projected on the macro time-scale ($L \cdot T$) more significantly than that projected on the micro time-scale (T). The larger influence of the capacity on the SOC leads to the possibility of more stable capacity estimation, and that is precisely the main technical characteristic that distinguishes our approach from the dual EKF.

6. SIMULATION AND EXPERIMENTAL RESULTS

The verification of the proposed multiscale framework was accomplished by conducting an extensive urban dynamometer drive schedule (UDDS) test. In Section 6.1, the synthetic data using a valid dynamic model of a high power LiPB cell are used to verify the effectiveness of the multiscale framework. Section 6.2 reports the results of UDDS cycle life test on Li-ion prismatic cells.

6.1 SOC and Capacity Estimation with Synthetic Data of High Power Cell

Synthetic Data Generation

In order to evaluate the performance of our proposed approach, we generated the synthetic data (T = 1s) using an ESC model of a prototype LiPB cell with a nominal capacity of 7.5Ah (Plett, 2006b). The root-mean-square (RMS) modeling error compared to cell tests was reported to be less than 10mV (Plett, 2004b). A sequence of 15 urban dynamometer driving schedule (UDDS) cycles (see Figure 3a), separated by 30A constant current discharge and 5min rest, result in the spread of SOC over the 100%-4% range (see Figure

3b). To account for the measurement error, the current and voltage data were contaminated by zero mean Gaussian noise with standard deviations 200mA and 10mV, respectively.

Capacity Estimation Results

To test the performance of the dual EKF and the multiscale framework with EKF, we intentionally offset the initial capacity value (7.0Ah) from the true value (7.5Ah). The results of capacity estimations by these two methods are summarized in Figure 3c and 3d, respectively, from which three important observations can be made. First of all, both methods produced converged capacity estimates with identical similar convergence rate. Indeed, the convergence rate can be adjusted by varying the process and measurement noise covariances which, respectively, represent the process uncertainty resulting from the model inaccuracy and the measurement uncertainty resulting from external disturbance that corrupts the measurement data. Secondly, the dual EKF yielded inaccurate and noisy capacity estimation (see Figure 3c) while the multiscale framework (L = 100) with EKF produced more accurate and stable capacity estimation (see Figure 3d). This can be attributed to the fact that the state projection in Eq. (30) magnifies the effect of the capacity on the SOC as well as removes to some extent the measurement noise. To minimize the effect of randomness in measurement noise, we repeated this simulation process ten times and obtained average RMS capacity estimation errors after convergence (at t = 200mins) to be 0.048Ah (relative error 0.640%) and 0.033Ah (relative error 0.440%) for the dual EKF and the multiscale framework with EKF, respectively. Thirdly, it is observed that, although the multiscale framework with EKF produced stable capacity estimation, the estimate still exhibits small fluctuation over time. It is fair to say, however, that the small noise does not really affect the practical use of this estimate.

Computational Efficiency

In the previous subsection, we have demonstrated that the proposed multiscale framework yielded higher accuracy than the dual EKF. In this subsection, we compare the two methods in terms of computational efficiency. To minimize the effect of randomness in measurement noise, we employed the ten synthetic data sets with each being executed ten times. Our computations were carried out on a processor Intel Core i5 760 CPU 2.8GHz and 4 GByte RAM. The codes for both methods were self-devised hand-optimized MATLAB codes running in Matlab environment (MATLAB Version 7.11.0.584, The MathWorks, Inc., Natick, MA USA).

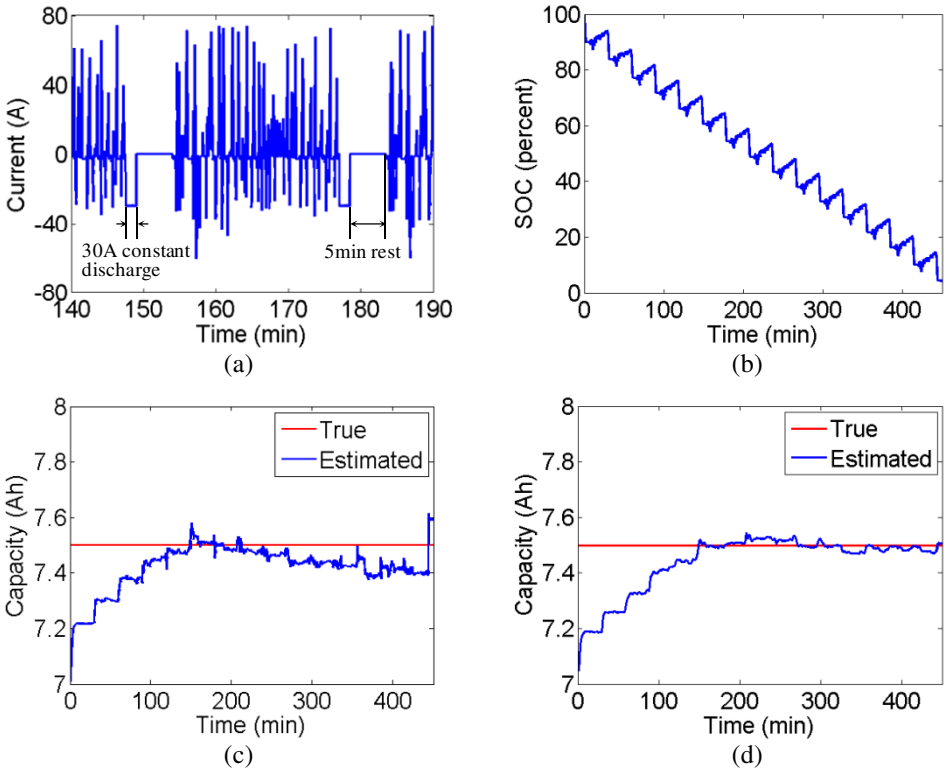

Figure 3: Synthetic data and results of capacity estimation. Figure (a) plots the rate profile for one UDDS cycle and (b) plots the SOC profile; (c) and (d) plot the results of capacity estimation by dual EKF and multiscale framework with EKF, respectively.

To make our comparison of general use to other engineering systems, we ruled out the computational time required to execute the ESC model in this study. In fact, the measurement functions of two engineered systems may exhibit a large difference in the level of complexity, resulting in different amounts of computational time. Thus, we intend to minimize the effect of system-to-system variation and focus on the general functions in an EKF by assuming a negligibly small amount of time for the execution of the system-specific measurement function (ESC model).

Table 3 summarizes the mean computational times. It is observed that the multiscale framework with EKF requires a smaller amount of computational time of 1.456s for the sequence of 15 UDDS cycles, a 34.145% reduction over the dual EKF whose computational time is 2.210s. Note that the percent of improvement is less than 50%. This can be attributed to the following two reasons: (i) from the standpoint of computations on the micro time-scale, it is noted that, in addition to the time- and measurement-update computations for SOC estimation, both methods also require the recursive derivative computation which, to some extent, reduces their efficiency gap; and (ii) from the standpoint of computations on the macro time-scale, although the macro-EKF is executed only upon the completion of L = 100 executions of the micro-EFK, it still requires a certain amount of time to compute the time- and measurement-updates for capacity estimation. In spite of these points, it is fair to say, however, that the proposed method achieves considerable improvement over the dual EKF in terms of computational efficiency. This improvement is critical to alleviating the computational burden imposed on the hardware and thus enhancing the feasibility of applications.

Table 3 Comparison results of computation efficiency with ten synthetic data sets

Method	Computational time (s)	Improvement (%)
Dual EKF	2.210	---
Mutiscale EKF	1.456	34.145

6.2 SOC and Capacity Estimation with UDDS Cycle Life Test of a Prismatic Cell

Description of Test Procedure

In addition to the numerical study using synthetic data, we also conducted the UDDS cycle test to verify the effectiveness of the multiscale framework. The cycle test data were extracted from an accelerated life test (ALT) that is currently being performed on sixteen 1500-mAh Li-ion prismatic cells. We set up a UDDS test system (see Figure 4) which comprises of an MACCOR Series 4000 cycle tester with a data acquisition device, an Espec SH-241 temperature chamber and a test jig as a connector holder for prismatic cells. Sixteen prismatic cells were placed in the temperature chamber and held by the test jig throughout the test.

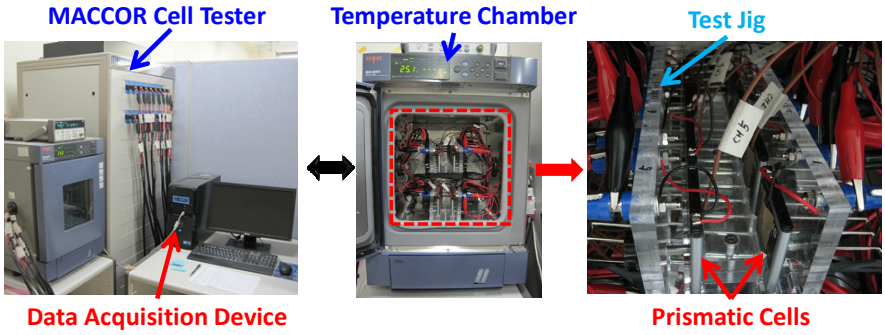

Figure 4: Experiment setup – UDDS cycle life test system.

All cycling experiments were performed at a constant room temperature, i.e., 25˚C. A two-level design of experiment (DOE) was used to study the effects of charging and discharging conditions on the health degradation. With two levels for charging conditions (1.0C and 1.5C) and discharging conditions (1.0C and 2.0C), we have four experimental settings as shown in Table 4. Based on the cell degradation data obtained from tests, we will develop real-time SOH and SOL prediction algorithms. Figure 5 shows the detailed test procedure. After every 10 charging and discharging cycles with specified rates in Table 4, cells are tested with 10 urban dynamometer drive schedule (UDDS) cycles for algorithm verification, followed by a small rate (0.05C) constant discharge for capacity check.

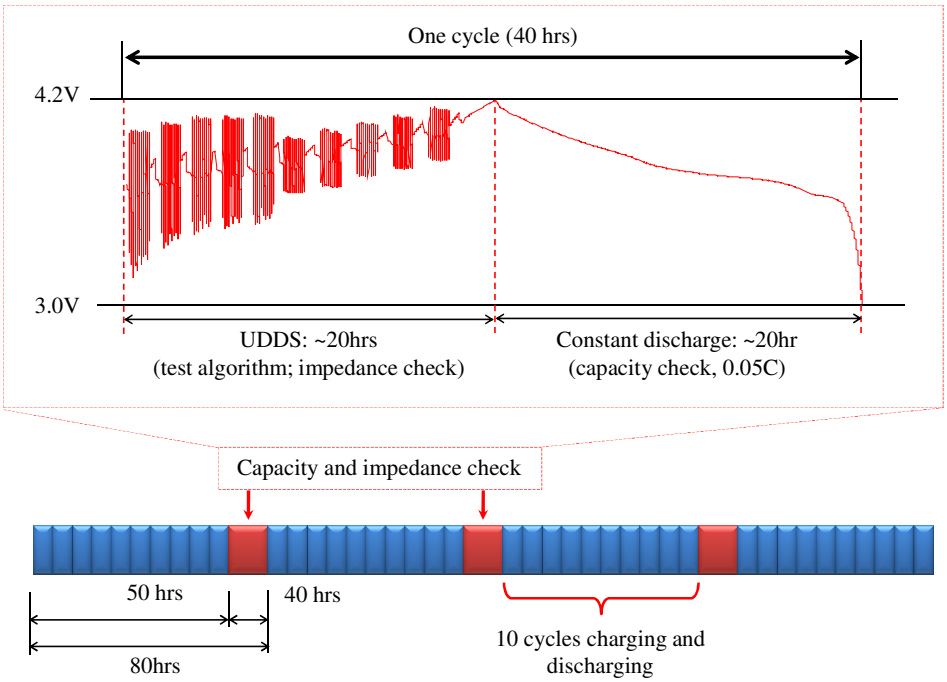

Figure 5: Detailed test procedure.

Table 4 Experiment settings

Charging Rate	Discharging Rate	Number of Cells
1.0C	1.0C	4
1.5C	1.0C	4
1.0C	2.0C	4
1.5C	2.0C	4

The capacity degradation of the 1500-mAh prismatic Li-ion cells under the first cycling condition in Table 3 is plotted in Figure 6. Under this condition, the cell capacity exhibits a linear relationship with the number of cycles and decreases by about 0.1Ah (6.5%) after 200 charging and discharging cycles. In what follows, we do not intend to investigate how to utilize this degradation behavior for SOL prediction but to employ the UDDS cycle test data before the cycling (1.0C charging, 1.0C discharging) from the first two cells to verify effectiveness of the proposed multiscale framework. The cycle test (see Figure 7a) is composed of 10 UDDS cycles, separated by 1C constant charge for 18 min and 18 min rest. This test profile resulted in the spread of SOC over the 4%-100% range. The SOC profile for 10 UDDS cycles is plotted in Figure 7b, where the SOC increases by about 9% during each charge period between cycles.

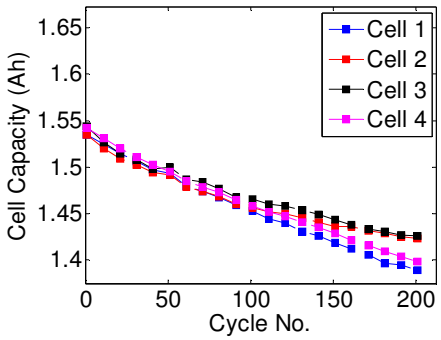

Figure 6: Capacity degradation under 1.0C charging rate and 1.0C discharging rate.

Training of ESC Cell Model

The current and voltage measurements of Cell 1 were used to train the ESC model (Plett, 2004a) while Cell 2 was treated as the testing cell. We followed the procedures described in (Plett, 2005) to obtain the open circuit voltage (OCV) curve. Through numerical optimization, optimum ESC model parameters were obtained which minimize the root mean squared (RMS) error of cell terminal voltage. The numerical optimization was performed using with a sequential quadratic programming (SQP) method. We employed a nominal capacity of 1.5Ah, a measurement interval of $T \approx 1$s, and four filter states $n_f = 4$. The voltage modeling results for one UDDS cycle are shown in Figure 8, where a good agreement can be observed.

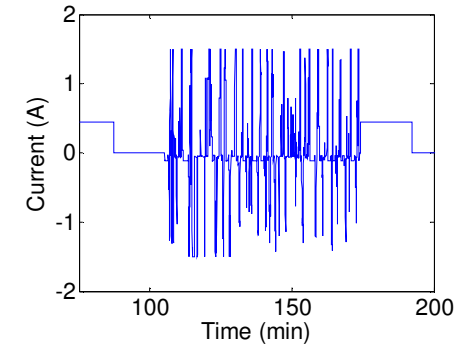

(a)

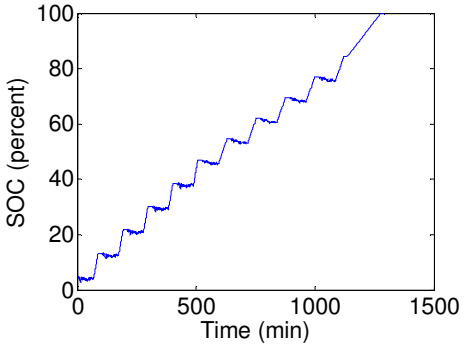

(b)

Figure 7: SOC profile and one cycle rate profile for UDDS cycle test. Figure (a) plots the rate profile for one UDDS cycle and (b) plots the SOC profile for 10 UDDS cycles.

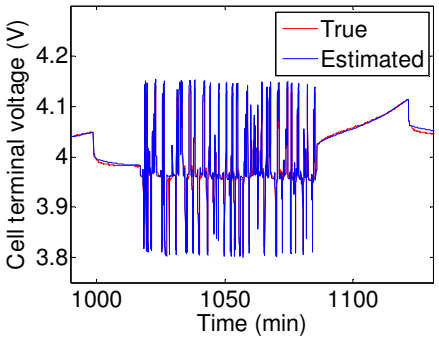

Figure 8: Modeled and measured cell terminal voltage for one UDDS cycle.

SOC and Capacity Estimation Results

The SOC estimation results for the training cell are shown in Figure 9, where we observe accurate SOC estimation produced by the multiscale framework (L = 1200). Table 5 summarizes the SOC estimation errors under two different settings of the initial SOC. Here, the RMS and maximum errors take into account the initial offset in the case of an incorrect initial SOC and are formulated as

$$\varepsilon_{RMS} = \sqrt{\frac{1}{nm}\sum_{k,j}\left(\hat{x}_{k,l} - x_{k,l}\right)^2}, \qquad \varepsilon_{Max} = \max_{k,j}\left|\hat{x}_{k,l} - x_{k,l}\right|. \tag{32}$$

where nm is the number of measurements and reads 69,173 (about 1290mins) in this study; and $x_{k,l}$ is the true SOC at the time $t_{k,l}$ estimated with the coulomb counting technique. It is observed that the RMS SOC estimation errors produced by the multiscale framework are less than 4.00%, regardless of initial values of the SOC. As expected, the SOC estimation with incorrect initial SOC (20%) shows larger errors than those with correct initial SOCs (4.84% and 4.77% for Cells 1 and 2, respectively). However, the RMS SOC estimation errors with incorrect initial SOC (20%) are still less than 4.00% since the multiscale framework produced converged SOC estimate for both cases.

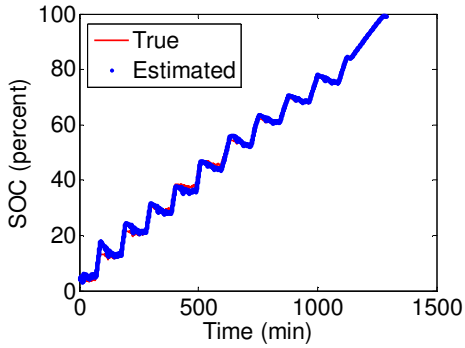

Figure 9: Estimated and true SOC estimate for 10 UDDS cycles.

Table 5 SOC estimation results under different settings of initial SOC and capacity

Initial SOC	SOC errors	Cell 1	Cell 2
Correct (4.84% and 4.77% for Cells 1 and 2)	RMS (%)	1.21	1.22
	Max (%)	4.58	4.95
Incorrect (20%)	RMS (%)	3.79	3.65
	Max (%)	15.16	15.23

Regarding the capacity estimation, both results with initial values smaller than the true value (see Figure10a) and larger than the real value (see Figure10b) for all the two cells exhibit convergence to the true capacity within an error range of around 5%. The noise in the capacity estimate is due to the SOC estimation error. We note that the time-scale separation in the SOC and capacity estimation enables converged capacity estimation in spite of SOC estimation error.

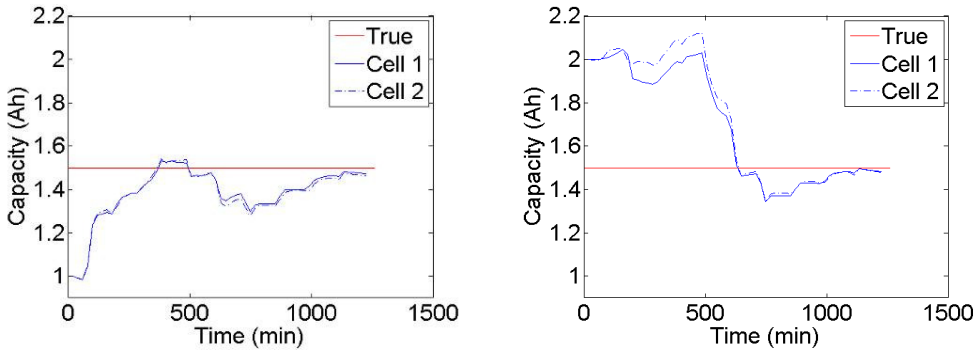

(a) (b)

Figure 10: Capacity estimation results for UDDS cycle test. Figures (a) and (b) plot capacity estimation results by the multiscale framework with the initial values smaller than and larger than the true value, respectively.

7. CONCLUSION

This paper presents a multiscale framework with EKF to efficiently and accurately estimate state and parameter for engineered systems that exhibit time-scale separation. We applied the proposed framework applied to the Li-ion battery system for SOC (state) and capacity (parameter) estimation. The main contribution of this paper lies in the decoupling of the SOC and capacity estimation from two perspectives, namely the measurement and time-scale, through the construction of a multiscale computational scheme. The resulting benefits are the significant reduction of the computational time as well as the increase of the accuracy in the capacity estimation. The former benefit makes the proposed methodology more attractive than the dual EKF for onboard estimation devices where the computational efficiency is the key aspect for practical use. Results from UDDS simulation and testing verify the effectiveness of the proposed framework for SOC and capacity estimation. As mentioned in Section 6.2, we are currently conducting ALTs (cell aging tests) on 16 Li-ion prismatic batteries. Based on the upcoming testing results, we aim to extend the proposed multiscale framework for efficient and accurate SOL prediction based on readily available measurements in a dynamic environment (e.g., UDDS cycling).

ACKNOWLEDGMENT

The authors gratefully acknowledge PCTEST Engineering Laboratory Inc. for providing testing facilities and Prof. Gregory L. Plett for providing the UDDS profile for this research.

NOMENCLATURE

C	cell capacity
$\mathbf{F}$	state transition function
$\mathbf{G}$	state measurement function
i	current
L	number of micro steps in a macro time step
$\mathbf{r}$	vector of process noise for model parameters
T	time between micro time step
x	cell state of charge
y	cell terminal voltage
$\mathbf{u}$	vector of observed exogenous inputs
$\mathbf{v}$	vector of measurement noise
$\mathbf{w}$	vectors of process noise for states
η	columbic efficiency
EKF	extended Kalman filter
HEV	hybrid electric vehicle
SOC	state of charge
SOH	state of health
SOL	state of life

REFERENCES

Plett, G.L. (2004a). Extended Kalman filtering for battery management systems of LiPB-based HEV battery packs Part 3. State and parameter estimation, *Journal of Power Sources*, vol. 134, no. 2, pp. 277–292.

Plett, G.L. (2006a). Sigma-point Kalman filtering for battery management systems of LiPB-based HEV battery packs Part 2: Simultaneous state and parameter estimation, *Journal of Power Sources*, vol. 161, no. 2, pp. 1369–1384.

Lee, S., Kim, J., Lee, J. & Cho, B.H. (2008). State-of-charge and capacity estimation of lithium-ion battery using a new open-circuit voltage versus state-of-charge, *Journal of Power Sources*, vol. 185, no. 2, pp. 1367–1373.

Zhang, Q. & White, R.E. (2008a). Capacity fade analysis of a lithium ion cell, *Journal of Power Sources*, vol. 179, no. 2, pp. 793–798.

Zhang, Q. & White, R.E. (2008b). Calendar life study of Li-ion pouch cells Part 2: Simulation, *Journal of Power Sources*, vol. 179, no. 2, pp. 785–792.

Saha, B., Goebel, K., Poll, S. & Christophersen J. (2009). Prognostics methods for battery health monitoring using a Bayesian framework, *IEEE Transaction on Instrumentation and Measurement*, vol. 58, no. 2, pp. 291–296.

Saha, B. & Goebel, K. (2009). Modeling Li-ion battery capacity depletion in a particle filtering framework, *In Proceedings of Annual Conference of the PHM Society*, San Diego, CA, Sep. 27-Oct. 1.

Plett, G.L. (2004b). Extended Kalman filtering for battery management systems of LiPB-based HEV battery packs Part 2. Modeling and identification, *Journal of Power Sources*, vol. 134, no. 2, pp. 262–276.

Plett, G.L. (2006b). Sigma-point Kalman filtering for battery management systems of LiPB-based HEV battery packs Part 1: Introduction and state estimation, *Journal of Power Sources*, vol. 161, no. 2, pp. 1356–1368.

Haykin, S. (2001). *Kalman Filtering and Neural Networks*, Wiley/Inter-Science, New York.

Wan, E. & Nelson, A. (2001). *Dual extended Kalman filter methods*, in: Haykin S. (Ed.), *Kalman Filtering and Neural Networks*, Wiley/Inter-Science, New York, p123–174.

Williams, R.J. & Zipser, D. (1989). A learning algorithm for continually running fully recurrent neural networks, *Neural Computation*, vol. 1, no. 2, pp. 270–280.

Plett, G. (2005). Results of temperature-dependent LiPB cell modeling for HEV SOC estimation, *In Proceedings of the 21st Electric Vehicle Symposium (EVS21)*, Monaco, April 2-6.

Chao Hu: Mr. Hu received his B.E. degree in Engineering Physics from Tsinghua University (Beijing, China) in 2003. He is currently pursuing the Ph.D. degree in mechanical engineering at The University of Maryland, College Park (Maryland, USA). His research interests are system reliability analysis, prognostics and health management (PHM), and battery power and health management of Li-ion battery system.

Byeng D. Youn: Dr. Byeng D. Youn is currently an Assistant Professor in the School of Mechanical and Aerospace Engineering at Seoul National University in South Korea. Dr. Youn is dedicated to well-balanced experimental and simulation studies of system analysis and design and is currently exploring three research avenues: (1) system risk-based design, (2) prognostics and health management (PHM), and (3) energy harvester design. Dr. Youn's research and educational portfolio includes: (i) *six notable awards***,** including the ISSMO/Springer Prize for the Best Young Scientist in 2005 from the International Society of Structural and Multidisciplinary Optimization (ISSMO), (ii) *over one hundred publications* in the area of system risk assessment and design and PHM. His primary applications include Li-ion batteries, consumer electronics, and large-scale engineered systems (e.g., automotives).

Taejin Kim: Mr. Kim received his B.E. degree in the School of Mechanical and Aerospace Engineering at Seoul National University (Seoul, Korea) in 2011. He is currently pursuing the M.S. degree in mechanical engineering at Seoul National University (Seoul, Korea). His research interests are prognostics and health management (PHM) for smart plant, and battery thermal and health management of Li-ion battery system.

Jaesik Chung: Dr. Chung, CTO of PCTEST, has managed the battery safety and reliability laboratory in PCTEST since 2007 in the business area of battery test, certification, safety project and R&D project relate to the battery safety and reliability. Before he joined PCTEST, he had worked for nineteen year in the area of electrochemical systems and Li–ion battery safety and reliability. He has managed a battery pack R&D team for his last eight years and developed smart battery algorithms and battery packs for mobile phones, notebook PCs, power tools, and mobility products and performed cell and battery pack safety designs for Apple, Dell, HP, IBM, Nokia, Motorola, Sony and other system makers.